

Full characterisation of polarisation states of light via direct measurement

Jeff Z. Salvail,¹ Megan Agnew,¹ Allan S. Johnson,¹ Eliot Bolduc,¹ Jonathan Leach,¹ Robert W. Boyd^{1,2}

¹*Dept. of Physics, University of Ottawa, Ottawa, Canada and*

²*Institute of Optics, University of Rochester, Rochester, USA*

(Dated: May 9, 2022)

Ascertaining the physical state of a system is vital in order to understand and predict its behaviour. Tomography is a standard approach used to determine the form of an unknown state. Here we show that an alternative approach, based on sequential weak and strong measurements, can be used to determine the density matrix in a simple, fast, and general style. We directly measure the probability amplitudes of a variety of pure polarisation states of light. We then generalise this experiment to directly measure the Dirac distribution and consequently determine the density matrix. Our work is the first to demonstrate the direct measurement of the full description of the state of a two-dimensional system, and it has applications to measurements in foundational quantum mechanics, quantum information, and physical chemistry.

Introduction.— Measurement plays a vital role in the practice of science. This is especially so in the case of quantum mechanics, where the measurement process plays a fundamental role in the formulation of the theory. A crucial feature of quantum mechanics is that a measurement of a variable of a system erases information about the corresponding conjugate variable. The classic example is that determining the position of a particle disturbs its momentum, and vice versa. These measurements, known as strong measurements, collapse the wavefunction such that no additional information can be obtained.

In order to completely determine a quantum state, which is described in general by complex numbers, one must perform multiple measurements on many identical copies of the system. Quantum tomography [1], proposed in 1957 [2], is one method of quantum state determination that uses strong measurements [3–7]. Tomographic reconstruction entails estimating the complex numbers that describe the state from the real-valued probabilities that result from strong measurements. Consequently, this approach can be considered *indirect* state determination due to the requirement of post-processing.

The first demonstration of *direct* quantum wavefunction measurement was recently reported [8]. In contrast to tomography, this method is considered direct because the measurement apparatus records the complex probability amplitudes describing the state. A recent proposal outlined how to generalise the technique to measure all aspects of a quantum state [9]. Although familiar and convenient, the density matrix is not the only way to describe a general quantum state. A state can be expressed in terms of its Dirac quasi-probability distribution (or phase-space representative), which is informationally equivalent to the density matrix ρ [10, 11]. For the direct measurement of a quantum state, the Dirac distribution is a convenient representation as its elements can be written simply in terms of weak values.

Directly measuring a quantum system relies on the technique of weak measurement: extracting so little in-

formation from a single measurement that the state does not collapse [12–26]. The first measurement of a weak value was the amplified the transverse displacement between the polarisation components of light induced by a birefringent crystal [15]. More recently, the technique was used to observe the transverse displacement a beam of light by only several angstroms [21] and an angular rotation on the order of femtoradians [22]. Weak measurement was recently proposed as a tool to study nonlinear optical phenomena with single photons by amplifying the apparent photon number [25]. Weak measurements have also allowed observation of apparent super-luminal velocity [17] and the mapping of average photon trajectories after they pass through a double slit [24].

The main result of our paper is the implementation of a procedure for the direct measurement of the polarisation state of coherent light. We demonstrate direct wavefunction measurement in a two-dimensional Hilbert space by weakly coupling the polarisation state of light to the spatial degree of freedom. We obtain the weak value by introducing a small spatial shift between the horizontal and vertical polarisation components, then strongly measuring the polarisation in the diagonal/anti-diagonal basis. Measurement of the mode’s position and momentum is performed to read out the real and imaginary components, respectively, of the weak value. By means of the weak values, we report the direct measurement of the polarisation wavefunction [8]. In a separate experiment, by means of the weak values and associated probabilities, we report the direct measurement of the polarisation Dirac distribution [9]. We show that for the case of a pure state qubit, measuring a single weak value completely determines the state. The description of the polarisation state of light is the same in the classical and quantum regimes; thus, we choose to perform our experiment with classical light. This study extends previous work on polarisation weak measurements [13, 15, 20].

Theory.— In any quantum measurement, the observer couples an unknown probe state to a pointer that reads

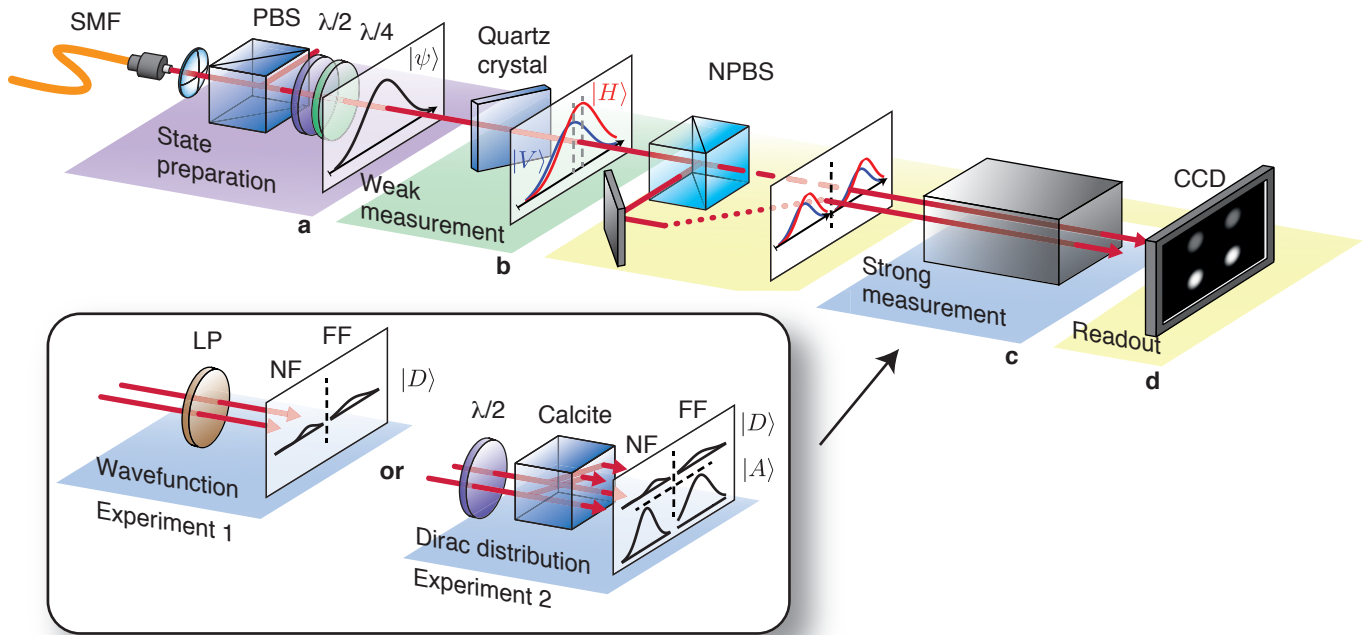


FIG. 1: Schematic representation of the experiment. **State Preparation (a):** The output of the single-mode fibre (SMF) is a near-Gaussian transverse mode of light. A polarising beamsplitter (PBS) and waveplate(s) create a known pure polarisation state. **Weak Measurement (b):** A quartz crystal at an oblique angle performs the weak measurement by introducing a small (compared to the beam waist) lateral displacement between horizontal and vertical polarisation components. **Strong Measurement (c):** A strong measurement in a basis mutually unbiased (diagonal/anti-diagonal) from the weak measurement is used to complete the direct measurement. **Inset:** To measure the wavefunction, a linear polariser oriented to transmit diagonally polarised light performs the strong measurement and post-selection; to measure the Dirac distribution, a $\lambda/2$ waveplate and calcite beam displacer perform the strong measurement. **Readout (d):** A 50:50 non-polarising beam splitter (NPBS) splits the light into two sub-ensembles. These are imaged in the near-field (dotted line, NF) and far-field (dashed line, FF) of the quartz crystal onto non-overlapping regions of the CCD camera.

out the value. For example, a birefringent crystal can couple the polarisation state of light to the spatial degree of freedom; in this case, the initial polarisation state is called the probe state, and the spatial degree of freedom of the light is considered the pointer. If the pointer state is a Gaussian mode with width w , a strong measurement separates the eigenstates of the measurement operator \hat{A} , by an amount $\delta \gg w$, such that the eigenstates are completely resolved.

Weak measurements occur in the opposite regime, where the coupling is much less than the pointer width $\delta \ll w$. In this case, the eigenstates of \hat{A} are not resolved by the pointer, so the wavefunction does not collapse. Therefore, a subsequent measurement performed on the quantum state can be used to extract further information. If the subsequent measurement is strong, such that the eigenstates are resolved, we can choose to consider only the statistics of one particular outcome; this is called post-selection and the chosen outcome of interest is the post-selected state. The result of the weak measurement

is called the weak value and is given by

$$\langle \hat{A} \rangle_{\phi}^w = \frac{\langle \phi | \hat{A} \rho | \phi \rangle}{\langle \phi | \rho | \phi \rangle}, \quad (1)$$

where ρ is the density operator that describes the initial state and $|\phi\rangle$ is the final, post-selected, state [16, 19]. In the case that the initial state is pure and may be described by the state vector $|\psi\rangle$ (i.e., $\rho = |\psi\rangle\langle\psi|$), the weak value in equation (1) simplifies to the form first introduced by Aharonov, Albert, and Vaidman [12]:

$$\langle \hat{A} \rangle_{\phi}^w = \frac{\langle \phi | \hat{A} | \psi \rangle}{\langle \phi | \psi \rangle}. \quad (2)$$

In the case that $|\psi\rangle = |\phi\rangle$, the expectation value of the weak measurement is equal to the standard expectation value of the operator \hat{A} . In general, the initial and final states may differ, and the weak value can be complex. For the specific case where the initial and final states are nearly orthogonal, the weak value can become arbitrarily large, leading to the amplification effect discussed above. The complex nature of the weak value, combined with

the fact that weak measurement does not significantly disturb the system, enables the direct measurement of the quantum state via weak measurements.

The complex weak value is determined by characterising the pointer. The pointer's position indicates the real part of the weak value $\text{Re}[\langle \hat{A} \rangle_\phi^W]$, and the pointer's momentum indicates the imaginary part $\text{Im}[\langle \hat{A} \rangle_\phi^W]$ [27].

In the specific case that the weak and final measurements are of mutually unbiased variables, the weak values have a direct relationship to the state description. The coefficients c_i of a wavevector $|\psi\rangle$ that describes a pure quantum state can be written in terms of specific weak values:

$$c_i = \langle a_i | \psi \rangle = \nu \langle \pi_{a_i} \rangle_{b_j}^W. \quad (3)$$

Here the weak measurement operator $\pi_{a_i} = |a_i\rangle\langle a_i|$ is the projector into the i^{th} state of the basis \mathcal{A} [8]. The factor ν is a constant of normalisation independent of i , which may be taken to be real. Equation (3) shows that the wavefunction describing a pure state can be directly measured by scanning weak measurements in basis \mathcal{A} and post-selecting on a fixed state in the mutually unbiased basis \mathcal{B} , then normalising the wavefunction.

An extension of the procedure that uses equation (3) gives a technique to directly measure the most general description of the quantum state. The simplest such generalisation entails measuring weakly in basis \mathcal{A} , followed by recording the results of all outcomes of the strong measurement in basis \mathcal{B} . In terms of the density operator ρ , the elements of the Dirac distribution that describes a general quantum state can be written in terms of specific weak values:

$$S_{ij} = \langle b_j | a_i \rangle \langle a_i | \rho | b_j \rangle = p_{b_j} \langle \pi_{a_i} \rangle_{b_j}^W. \quad (4)$$

That is to say, the $(i, j)^{\text{th}}$ element of the Dirac distribution is equal to the result of the weak measurement of π_{a_i} followed by post-selection on state b_j , multiplied by the probability of successful post-selection $p_{b_j} = \langle b_j | \rho | b_j \rangle$ [9]. Importantly, one can always invert equation (4) and calculate the density matrix ρ from the measured Dirac distribution S . For further details on equations (3) and (4), see the Supplementary Information.

Experiment.— We perform two experiments. First, we implement the technique encapsulated by equation (3) to measure a variety of pure polarisation wavefunctions. Second, we apply the technique encapsulated by equation (4) to measure the Dirac distribution of a variety of states. The only difference between the two experiments is in the nature of the strong measurement: in the first experiment, a single strong measurement outcome is required; whereas in the second experiment, all eigenstates of the strong measurement are recorded.

A brief summary of the experimental procedures is as follows; see Fig. 1 for a schematic. First, the probe (polarisation) and pointer (spatial mode) states are prepared

(a). Second, the weak measurement is performed by a quartz plate, which slightly displaces the two orthogonal polarisation components $|H\rangle$ and $|V\rangle$ of the probe laterally (b). Third, the strong measurement in the D/A basis is performed (c). To measure the wavefunction, we post-select the final state by projecting the polarisation into the diagonal state $|D\rangle$ using a linear polariser (LP) oriented to transmit diagonally polarised light. To measure the Dirac distribution, a calcite crystal separates the components $|D\rangle$ and $|A\rangle$ so that they do not overlap. Finally, the wavefunction or Dirac distribution is read out by imaging the near- and far-fields of the plane immediately after the quartz onto separate regions of interest of a CCD camera (d). Two regions are used to read out the wavefunction and four are needed to read out the Dirac distribution.

In order to demonstrate our ability to perform the direct measurement of the polarisation state, we measured the probability amplitudes of three sets of input polarisation states, each corresponding to a different great circle on the Poincaré sphere. The states were created by appropriate orientation of a half-wave plate and optionally, a quarter-wave plate. In the second experiment, we create a number of states in the same fashion and measure their Dirac distributions, then calculate the associated density matrix.

Results.— Figure 2 shows the measured weak values and corresponding polarisation probability amplitudes as a function of input polarisation angle. Figure 3 shows the calculated Stokes parameters for each measured $|\psi\rangle$ in Fig. 2 (blue points). We also show calculated Stokes parameters for two additional paths around the Poincaré sphere. Measured weak values and probability amplitudes are included in the supplementary materials for all these states.

Figure 4 shows directly measured Dirac distributions and the corresponding density matrices of different polarisation states. A variety of states are created for calibration as in the first experiment, but here all outcomes of the strong measurement are considered.

Discussion.— Figure 2 shows that the largest divergence between theory and result in experiment 1 occurs when the initial state is anti-diagonal and therefore orthogonal to the post-selected state of diagonal. In this limit, the weak value is undefined, whereas the pointer reaches a maximum displacement (see [12, 28]). This difficulty is overcome by the full state characterization technique performed in experiment 2. Recalling equation (4), it is precisely in this regime where p_{b_j} goes to zero, cancelling the effect of the breakdown of the weak-value approximation.

We note that density matrices determined by the technique demonstrated herein are not guaranteed to be precisely Hermitian due to measurement noise. For example,

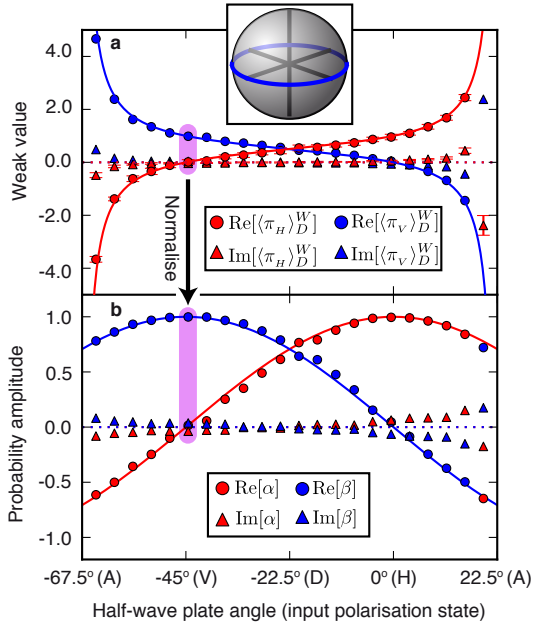


FIG. 2: Results of experiment 1 with linearly polarised probe states. **(a)** Measured weak values plotted as a function of input polarisation angle. Error bars are shown only for the red points for clarity. **(b)** Real and imaginary components of the probability amplitudes determined by normalising the weak values of each test state, where $|\psi\rangle = \alpha|H\rangle + \beta|V\rangle$. For both panels, the solid lines are the theoretical predictions of the real components, and the dotted lines are the theoretical predictions of the imaginary components. **Inset:** A Poincaré sphere with the path taken indicated by the blue line.

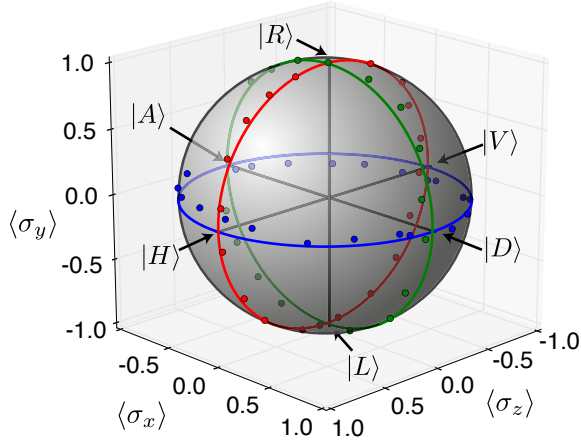


FIG. 3: Measured states on the Poincaré sphere. Here we show a Poincaré sphere with the set of directly measured states, indicated by their calculated Stokes parameters $\langle\sigma_x\rangle = \langle\psi|\pi_D - \pi_A|\psi\rangle$, $\langle\sigma_y\rangle = \langle\psi|\pi_R - \pi_L|\psi\rangle$, $\langle\sigma_z\rangle = \langle\psi|\pi_H - \pi_V|\psi\rangle$. The blue points indicate states created by rotating the half-wave plate. The red (green) points indicate calculated Stokes parameters for states created by rotating the half-wave plate, followed by a quarter-wave plate at fixed angle 0° (45°). The solid lines indicate the paths taken for each data set.

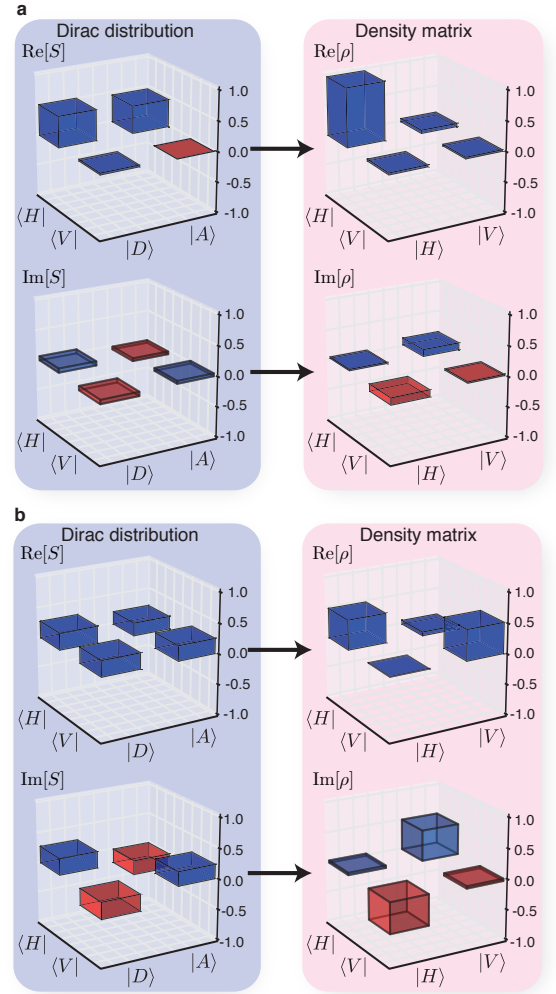


FIG. 4: Results of experiment 2. The directly measured Dirac distributions and corresponding density matrices for the horizontal linear polarisation state $|H\rangle$ (a) and left-hand circular polarisation state $|L\rangle = 1/2((1+i)|H\rangle + (1-i)|V\rangle)$ (b). The axes of the Dirac distribution are the mutually unbiased bases H/V and D/A ; the density matrix describes the state in terms of only one basis H/V .

the density matrices shown in Figure 4 have small imaginary components along the diagonal, of magnitude on the order of the measurement uncertainty ($\approx 3\%$).

The similarity between equations (3) and (4) suggests a simple connection between the coefficients of the wavefunction and the entries of its Dirac distribution. In the case that the state is pure, we may combine the two equations to determine the real constant of proportionality that relates the two:

$$c_i = \frac{\nu}{pb_j} S_{ij}. \quad (5)$$

We see that there is a column j of the Dirac distribution that is proportional to the wavefunction c_i . It is,

in particular, the column corresponding to the choice of post-selection in equation (3) that renders ν independent of i (and hence can be taken to be real).

Equation (5) has particular relevance to our experiment for the states that have a constant of normalisation ν equal to unity and a probability of post-selection equal to one half. These states lie on the great circle of the Poincaré sphere that includes $\{|H\rangle, |R\rangle, |V\rangle, |L\rangle\}$ (red points in Fig. 3, weak values and probability amplitudes in Fig. 5 in the Supplementary information). Each state on this circle is from a basis that is mutually unbiased with respect to the strong measurement π_D . For these states, we see that $c_i = 2S_{ij}$ and hence the wavefunction is twice a column of the Dirac distribution. See Figure 4 for two examples.

The technique we demonstrate compares favourably with quantum tomography with regards to inferring the density matrix from measurement results. Tomography via maximum likelihood estimation or least-squares fitting, which is an example of an inverse problem, becomes prohibitively difficult as the dimension of the state or number of particles in a multipartite state increases. The difficulty arises from the computational requirements of varying the vast number of fit parameters needed to estimate the state [7, 29]. In contrast, no fitting is required to determine the density matrix from the directly measured Dirac distribution because it is calculated analytically. Hence, we anticipate that for high-dimensional quantum systems especially, direct measurement will become a widely used technique for quantum state determination.

Conclusion.— In conclusion, we have performed direct measurements of general polarisation states of coherent light. We obtain our results through parallel measurements of the real and imaginary components of the weak value of polarisation. An important result is that a single weak value, corresponding to the weak measurement of only one observable, determines both complex coefficients of the pure state of a qubit. Our experiment was performed at classical light levels; however, this work paves the way for future direct measurement of discrete quantum systems.

We anticipate that the general method prescribed in this work will be applied to a variety of two-level systems. For example, the wavefunction or density matrix of polarisation-entangled photon pairs in quantum key distribution schemes and of spin qubits in quantum computing can be measured directly. If the calcite crystal in our second experiment is replaced with a second quartz plate as thin as the first, the density matrix of the ensemble can be determined with vanishingly small disturbance to its state before absorption by the camera. Indeed it should be possible, in principle, to measure the quantum state of an ensemble without destroying it, by weakly coupling the probe state of one particle to the pointer of

another as in Ref. [20]. This has implications for quantum protocols, as well as physical chemistry, where one can imagine determining the quantum state of an ensemble without affecting it significantly.

METHODS

A near Gaussian pointer state is prepared by passing HeNe laser light through a single mode fiber (SMF). The probe is then prepared by polarising the light with a polarising beam splitter (PBS) then rotating the angle of polarisation with a half-wave plate ($\lambda/2$) and/or quarter-wave plate ($\lambda/4$).

The weak measurement is performed by coupling polarisation information to the spatial degree of freedom of the light. Light incident at an oblique angle on an X -cut quartz crystal undergoes a polarisation-dependent parallel displacement. By aligning the extraordinary axis with the x -axis and rotating the crystal about the y -axis, horizontal and vertical polarisations become slightly separated in x . We take the z -axis to be the direction of propagation of the light, x to be the transverse direction parallel to the optical table, and y to be the transverse direction perpendicular to the table. The angle of incidence was adjusted to $\sim 40^\circ$ to ensure the two optical paths through the crystal are equal, mod 2π , through the ordinary and extraordinary axes (based on crystal thickness of 700 μm).

It is important that the pointer state be a Gaussian with a flat phase-front. We collect the SMF output with a microscope objective ($10\times$), and focus the light onto the quartz crystal (≈ 45 cm away). This ensures the phase-front is approximately flat over the region of interaction with the quartz.

After strong measurement, the real part of the weak value is proportional to the average position $\langle x \rangle$ of the post-selected intensity distribution immediately behind the quartz. The quartz plane is imaged onto the camera by two sets of relay optics. The first set images ($2f_1$ - $2f_2$ imaging system, $f_1 = 100$ mm, $f_2 = 125$ mm,) to a spatial filter (adjustable iris) that allows us to eliminate back-reflections created in the quartz crystal; the second set images ($2f_1$ - $2f_2$ imaging system, $f_1 = 75$ mm, $f_2 = 250$ mm,) the iris plane onto the camera. The imaginary part of the weak value is proportional to the average position of the intensity distribution in the far-field $\langle p_x \rangle$ of the quartz plane. A Fourier transform lens ($f = 300$ mm) maps the far-field distribution of the iris plane onto the camera.

We establish the expectation value of each pointer by first integrating each intensity distribution $I(x, y)$ along y to find $I(x) = \sum_{y \text{ pixels}} I(x, y) \Delta y$, followed by finding the average $\langle x \rangle = \sum_{x \text{ pixels}} x I(x) \Delta x / \sum_{x \text{ pixels}} I(x) \Delta x$. This procedure is repeated with the image of the far-field to establish $\langle p_x \rangle$, and for each strong measurement

outcome.

The expectation values $\langle x \rangle$ and $\langle p_x \rangle$ of the pointer, and their corresponding standard deviations, are established by averaging 100 CCD images, each with a 2000- μs exposure time. The only exception is for the data used to calibrate the weak values for Figure 4b, where we averaged over 50 CCD images, each with a 500- μs exposure time. This was to reduce the effect of spot drift over the course of the calibration run where many states are measured sequentially.

A simple background subtraction is performed before calculating the pointer's position and momentum. We subtract the value of the minimum pixel from all pixels on each exposure, to reduce the effect that the background has on calculating the average. For the post-selection probability measurements used to determine the Dirac distribution, background subtraction is performed for each region of interest by subtracting the recorded intensity when the laser is blocked. The intensity after background subtraction of the near-field image corresponding to the outcome $|D\rangle$ is I_D and of $|A\rangle$ is I_A . Thus the probabilities are calculated according to $p_D = I_D/(I_D + I_A)$ and $p_A = I_A/(I_D + I_A)$.

The weak value is obtained from average pixel number by

$$\langle \pi_H \rangle_D^W = a\langle x \rangle - b + i(c\langle p_x \rangle - d), \quad (6)$$

where a, b, c, d are constants that must be determined by calibrating the measurement apparatus. Another set of calibration constants a', b', c', d' must be determined for the post-selection of $|A\rangle$ to convert average pixel to $\langle \pi_H \rangle_A^W$. We perform calibrations of the measurement apparatus by measuring the wavefunctions and Dirac distributions of known pure states and comparing $\langle x \rangle$ and $\langle p_x \rangle$ to theoretically calculated weak values.

ACKNOWLEDGEMENTS

We thank K. Piché and F. Miatto for helpful discussions regarding this work. We thank P. B. Corkum and C. Zhang for lending us the quartz crystal. This work was supported by the Canada Excellence Research Chairs (CERC) Program.

AUTHOR CONTRIBUTIONS

The concept was devised by J. Z. S. The experiment was designed by J. Z. S., A. S. J., E. B., and J. L. The experiment was performed by J. Z. S., M. A., and A. S. J., and data analysis was performed by J. Z. S. All authors contributed to the text of the manuscript.

- [1] G. M. D'Ariano, M. G. A. Paris, and M. F. Sacchi, Quantum tomography, *Adv. Imaging Electron Phys.*, **128**, 205 (2003).
- [2] U. Fano, Description of states in quantum mechanics by density matrix and operator techniques, *Rev. Mod. Phys.*, **29**, 74 (1957).
- [3] K. Banaszek, G. M. D'Ariano, M. G. A. Paris, and M. F. Sacchi, Maximum-likelihood estimation of the density matrix, *Phys. Rev. A*, **61**, 010304 (1999).
- [4] A. G. White, D. F. V. James, W. J. Munro, and P. G. Kwiat, Exploring hilbert space: Accurate characterization of quantum information, *Phys. Rev. A*, **65**, 012301 (2001).
- [5] J. Itatani, J. Levesque, D. Zeidler, H. Niikura, H. Pépin, J. C. Kieffer, P. B. Corkum, and D. M. Villeneuve, Tomographic imaging of molecular orbitals, *Nature*, **432**, 867 (2004).
- [6] K. J. Resch, P. Walther, and A. Zeilinger, Full characterization of a three-photon greenberger-horne-zeilinger state using quantum state tomography, *Phys. Rev. Lett.*, **94**, 70402 (2005).
- [7] M. Agnew, J. Leach, M. McLaren, F. S. Roux, and R. W. Boyd, Tomography of the quantum state of photons entangled in high dimensions, *Phys. Rev. A*, **84**, 062101 (2011).
- [8] J. S. Lundeen, B. Sutherland, A. Patel, C. Stewart, and C. Bamber, Direct measurement of the quantum wavefunction, *Nature (London)*, **474**, 188 (2011).
- [9] J. S. Lundeen and C. Bamber, Procedure for direct measurement of general quantum states using weak measurement, *Phys. Rev. Lett.*, **108**, 70402 (2012).
- [10] P. A. M. Dirac, On the analogy between classical and quantum mechanics, *Rev. Mod. Phys.*, **17**, 195 (1945).
- [11] S. Chaturvedi, E. Ercolessi, G. Marmo, G. Morandi, N. Mukunda, and R. Simon, Wigner-Weyl correspondence in quantum mechanics for continuous and discrete systems—a Dirac-inspired view, *J. Phys. A*, **39**, 1405 (2006).
- [12] Y. Aharonov, D. Z. Albert, and L. Vaidman, How the result of a measurement of a component of the spin of a spin-1/2 particle can turn out to be 100, *Phys. Rev. Lett.*, **60**, 1351 (1988).
- [13] I. M. Duck, P. M. Stevenson, and E. C. G. Sudarshan, The sense in which a weak measurement of a spin-1/2 particle's spin component yields a value 100, *Phys. Rev. D*, **40**, 2112 (1989).
- [14] J. M. Knight and L. Vaidman, Weak measurement of photon polarization, *Phys. Lett. A*, **143**, 357 (1990).
- [15] N. W. M. Ritchie, J. G. Story, and R. G. Hulet, Realization of a measurement of a weak value, *Phys. Rev. Lett.*, **66**, 1107 (1991).
- [16] H. Wiseman, Weak values, quantum trajectories, and the cavity-QED experiment on wave-particle correlation, *Phys. Rev. A*, **65**, 032111 (2002).
- [17] D. R. Solli, C. F. McCormick, R. Y. Chiao, S. Popescu, and J. M. Hickmann, Fast light, slow light, and phase singularities: A connection to generalized weak values, *Phys. Rev. Lett.*, **92**, 043601 (2004).
- [18] K. J. Resch, J. S. Lundeen, and A. M. Steinberg, Experimental realization of the quantum box problem, *Phys. Lett. A*, **324**, 125 (2004).

- [19] L. Johansen, Weak Measurements with Arbitrary Probe States, *Phys. Rev. Lett.*, **93**, 120402 (2004).
- [20] G. J. Pryde, J. L. O’Brien, A. G. White, T. C. Ralph, and H. M. Wiseman, Measurement of quantum weak values of photon polarization, *Phys. Rev. Lett.*, **94**, 220405 (2005).
- [21] O. Hosten and P. Kwiat, Observation of the spin hall effect of light via weak measurements, *Science*, **319**, 787 (2008).
- [22] P. B. Dixon, D. J. Starling, A. N. Jordan, and J. C. Howell, Ultrasensitive beam deflection measurement via interferometric weak value amplification, *Phys. Rev. Lett.*, **102**, 173601 (2009).
- [23] S. Popescu, *Physics*, **2** (2009).
- [24] S. Kocsis, B. Braverman, S. Ravets, M. J. Stevens, R. P. Mirin, L. K. Shalm, and A. M. Steinberg, Observing the average trajectories of single photons in a two-slit interferometer, *Science*, **332**, 1170 (2011).
- [25] A. Feizpour, X. Xing, and A. M. Steinberg, Amplifying single-photon nonlinearity using weak measurements, *Phys. Rev. Lett.*, **107**, 133603 (2011).
- [26] M. A. de Gosson and S. M. de Gosson, Weak values of a quantum observable and the cross-Wigner distribution, *Phys. Lett. A*, **376**, 293 (2012).
- [27] J. S. Lundeen and K. J. Resch, Practical measurement of joint weak values and their connection to the annihilation operator, *Phys. Lett. A*, **334**, 337 (2005).
- [28] T. Geszti, Postselected weak measurement beyond the weak value, *Phys. Rev. A*, **81**, 044102 (2010).
- [29] M. Agnew, J. Leach, and R. W. Boyd, Observation of entanglement witnesses for orbital angular momentum states, *Eur. Phys. J. D*, **66**, 156 (2012).
- [30] W. K. Wootters and B. D. Fields, Optimal state-determination by mutually unbiased measurements, *Annals of Physics*, **191**, 363 (1989).

SUPPLEMENTARY INFORMATION

Mutually unbiased bases

Two bases \mathcal{A} and \mathcal{B} are said to be mutually unbiased if $|\langle a_i | b_j \rangle|^2 = 1/N$ for all states $|a_i\rangle$ in \mathcal{A} and all states $|b_j\rangle$ in \mathcal{B} , where N is the dimension of the Hilbert space in which $|\psi\rangle$ lives and upon which ρ operates [30]. The indices i and j take the integers from 0 to $N - 1$. For example, the horizontal/vertical polarisation basis $\mathcal{A} = \{|H\rangle, |V\rangle\}$ is mutually unbiased with respect to the diagonal/anti-diagonal polarisation basis $\mathcal{B} = \{|D\rangle = 1/\sqrt{2}(|H\rangle + |V\rangle), |A\rangle = 1/\sqrt{2}(|H\rangle - |V\rangle)\}$.

The wavefunction and weak values

We summarize the technique proposed and performed by Lundeen *et al.* in Ref. [8], where a spatial wavefunction of an ensemble of single photons was measured directly, using polarisation as the pointer.

Recall that any state $|\psi\rangle$ in the Hilbert space spanned

by \mathcal{A} can be written as

$$|\psi\rangle = \sum_i c_i |a_i\rangle, \quad (7)$$

where each $c_i \equiv \langle a_i | \psi \rangle$ is a probability amplitude that cannot be accessed directly by strong measurements. The set $\{c_i\}$ is the wavefunction of the state expressed in the \mathcal{A} basis.

Consider a weak measurement of the projection operator $\pi_{a_i} \equiv |a_i\rangle\langle a_i|$, and post-selection on a state $|\phi\rangle = |b_j\rangle$, where $|b_j\rangle$ and $|a_i\rangle$ are states in mutually unbiased bases. In this case, equation (1) gives the weak value

$$\langle \pi_{a_i} \rangle_{b_j}^W = \frac{\langle b_j | a_i \rangle \langle a_i | \psi \rangle}{\langle b_j | \psi \rangle} = \frac{1}{\nu} \langle a_i | \psi \rangle, \quad (8)$$

where ν is a constant of normalisation and is equal to

$$\nu = \frac{\langle b_j | \psi \rangle}{\langle b_j | a_i \rangle}. \quad (9)$$

Crucially, for the specific case where the weak and final measurements are mutually unbiased, the magnitude of the constant ν is independent of i . In general, only for one choice of $|b_j\rangle$ will the phase of ν be independent of i . This ensures that the weak values are proportional through ν to the complex probability amplitudes c_i . Thus, we can substitute the c_i in equation (7) with the normalised weak values from equation (8) to re-express the wavevector as

$$|\psi\rangle = \nu \sum_i \langle \pi_{a_i} \rangle_{b_j}^W |a_i\rangle. \quad (10)$$

Observation of the wavefunction is therefore performed by measuring each coefficient in turn and normalising the magnitude of the wavefunction to unity, which determines ν .

The wavefunction is determined by measuring the pointer state. The pointer’s position indicates the real part of the weak value $\text{Re}[\langle \pi_{a_i} \rangle_{b_j}^W]$, and the pointer’s momentum indicates the imaginary part $\text{Im}[\langle \pi_{a_i} \rangle_{b_j}^W]$ [27]. Returning to the example where the pointer is the spatial degree of freedom, the complex weak value $\langle \pi_{a_i} \rangle_{b_j}^W$ is established by measuring the expectation values $\langle x \rangle$ and $\langle p_x \rangle$ of the spatial mode: $\text{Re}[\langle \pi_{a_i} \rangle_{b_j}^W] = \langle x \rangle / \delta$ and $\text{Im}[\langle \pi_{a_i} \rangle_{b_j}^W] = k \langle p_x \rangle / \delta$. The constant of proportionality $k = 2\sigma^2 / \hbar$, with σ the beam waist, is related to the measurement backaction [27].

In our work, we make use of the fact that not all the weak values $\langle \pi_{a_i} \rangle_{b_j}^W$ are independent. Taking the sum of a complete set of weak values corresponding to projectors $|a_i\rangle\langle a_i|$ with fixed post-selection $|b_j\rangle$, we obtain unity:

$$\begin{aligned} \sum_{i=0}^{N-1} \langle \pi_{a_i} \rangle_{b_j}^W &= \sum_i \frac{\langle b_j | a_i \rangle \langle a_i | \rho | b_j \rangle}{\langle b_j | \rho | b_j \rangle} \\ &= \langle b_j | \left(\sum_i |a_i\rangle\langle a_i| \right) \frac{\rho | b_j \rangle}{\langle b_j | \rho | b_j \rangle} \\ &= 1. \end{aligned} \quad (11)$$

This result is true for any post-selection $|b_j\rangle = |\phi\rangle$ and relies on the fact that $\sum_i |a_i\rangle\langle a_i|$ is equal to the identity operator when the set of all $|a_i\rangle$ is a complete basis. Therefore, measuring all but one weak value is sufficient to determine the wavefunction. Importantly, for a qubit, a single weak value determines the pure state in the two-dimensional Hilbert space.

We now consider the direct measurement of the polarisation wavefunction of a photon. Although the context of our work is polarisation, these results are general and apply to all two-state quantum systems. The polarisation state of a photon can be written as a linear combination of basis elements

$$|\psi\rangle = \alpha|H\rangle + \beta|V\rangle, \quad (12)$$

where α, β are complex probability amplitudes, and $|\alpha|^2 + |\beta|^2 = 1$. Recalling equation (3), we may express the polarisation state as

$$|\psi\rangle = \nu (\langle\pi_H\rangle_D^W |H\rangle + \langle\pi_V\rangle_D^W |V\rangle), \quad (13)$$

where the post-selected state is $|D\rangle$, and therefore mutually unbiased with respect to the measurement operators $\pi_H = |H\rangle\langle H|$ and $\pi_V = |V\rangle\langle V|$. The constant ν is simply found by normalising the wavefunction and is equal to $(|\langle\pi_H\rangle_D^W|^2 + |\langle\pi_V\rangle_D^W|^2)^{-\frac{1}{2}}$. We now see that the wavefunction is defined in terms of quantities that we can directly measure in the lab. Equation (13) can be simplified by using the fact that $\langle\pi_V\rangle_D^W + \langle\pi_H\rangle_D^W = 1$ as in equation (11). Thus, we may eliminate $\langle\pi_V\rangle_D^W$, and the wavefunction is defined entirely in terms of $\langle\pi_H\rangle_D^W$.

The weak value $\langle\pi_H\rangle_D^W$ can be calculated from its definition (equation (1)) and the polarisation state (equation (12)):

$$\begin{aligned} \langle\pi_H\rangle_D^W &= \frac{\langle D|H\rangle\langle H|\psi\rangle}{\langle D|\psi\rangle} = \frac{\alpha}{\alpha + \beta} \\ &= \frac{\cos\theta}{\cos\theta + e^{i\varphi}\sin\theta}. \end{aligned} \quad (14)$$

We take the convention here that the horizontal component has a real coefficient, such that the coefficients are defined by $\alpha = \cos\theta$ and $\beta = e^{i\varphi}\sin\theta$, where θ is the polarisation angle and φ is the phase difference between components. The result of equation (14) can also be obtained through the methods of classical optics. The locations of the peaks of the intensity distributions obtained from the interference of two overlapping Gaussian modes, in the near- and far-fields, are proportional to the real and imaginary parts of equation (14), respectively [15]. In this representation, the two degrees of freedom of a polarisation qubit are θ and φ ; in terms of weak values, they are the independent real and imaginary parts of $\langle\pi_H\rangle_D^W$. Setting a convention such as this for the phase fixes the gauge, or reference frame, with respect to which the wavefunction is measured. Choosing

ν real actually sets a different phase convention, where the wavevector has an additional global phase coefficient $\exp(-i\arg[\alpha + \beta])$. We plot the wavefunctions in Fig. 2 using this phase convention, since it is the natural choice that comes from experiment. The theory curves of Figures 2, 5, and 6 are calculated according to equation (14) by setting $\varphi = 0, \pi/2, \pi/4$ respectively, then setting the wavefunction's phase as discussed above.

The Dirac distribution and weak values

We summarize the technique proposed by Lundeen and Bamber in Ref. [9]. The Dirac distribution, named for Dirac who proposed it in Ref. [10], is investigated thoroughly by Chaturvedi *et al.* in Ref. [11]. In our work, we use Chaturvedi *et al.*'s "left" phase-space representative (Dirac distribution) throughout, and discuss only the discrete (i.e., N -level) Hilbert space version.

The entry in the i^{th} row and the j^{th} column of the Dirac distribution of the state described by ρ is given by

$$S_{ij} = \langle b_j|a_i\rangle\langle a_i|\rho|b_j\rangle. \quad (15)$$

Recalling the weak value defined in equation (1), for weak measurement of a projector π_{a_i} , we obtain

$$\langle\pi_{a_i}\rangle_{b_j}^W = \frac{\langle b_j|\pi_{a_i}\rho|b_j\rangle}{\langle b_j|\rho|b_j\rangle} = \frac{\langle b_j|a_i\rangle\langle a_i|\rho|b_j\rangle}{\langle b_j|\rho|b_j\rangle}. \quad (16)$$

Substituting equation (16) into equation (15), we now see that the elements of the Dirac distribution that describes a general quantum state can be written in terms of particular weak values that can be directly measured:

$$S_{ij} = \langle b_j|\rho|b_j\rangle\langle\pi_{a_i}\rangle_{b_j}^W = p_{b_j}\langle\pi_{a_i}\rangle_{b_j}^W. \quad (17)$$

That is to say, the $(i, j)^{\text{th}}$ element of the Dirac distribution is equal to the result of the weak measurement of π_{a_i} with a post-selection on state b_j , multiplied by the probability of successful post-selection $p_{b_j} = \langle b_j|\rho|b_j\rangle$. The generalised technique uses the outcome of the strong measurement, and since a mixed state density matrix (and hence Dirac distribution) has more degrees of freedom ($N^2 - 1$) than a pure state vector ($2N - 2$), the strong measurement projection must be scanned through the basis \mathcal{B} , in addition to scanning the weak measurement through the complimentary basis \mathcal{A} .

To calculate the density matrix ρ from the Dirac distribution S , a simple row-by-row discrete Fourier transform can be used, since the H/V basis and D/A basis are not only mutually unbiased but Fourier bases. The relation is

$$\rho_{ij} = \sum_{k=0}^{N-1} S_{ik} \exp\left(\frac{2\pi i}{N}(i-k)j\right). \quad (18)$$

In equation (18), we use i to denote the imaginary unit which is distinct from the index i .

In terms of experiment outcomes, the Dirac distribution is

$$S = \left. \begin{array}{cc} p_D \langle \pi_H \rangle_D^W & p_A \langle \pi_H \rangle_A^W \\ p_D \langle \pi_V \rangle_D^W & p_A \langle \pi_V \rangle_A^W \end{array} \right\} \begin{array}{l} \text{Left basis axis } \langle H \rangle, \langle V \rangle \\ \text{Right basis axis } |D\rangle, |A\rangle \end{array} \quad (19)$$

Using equation (18) with $N = 2$, we obtain the density matrix

$$\rho = \begin{pmatrix} p_D \langle \pi_H \rangle_D + p_A \langle \pi_H \rangle_A & p_D \langle \pi_H \rangle_D - p_A \langle \pi_H \rangle_A \\ p_D \langle \pi_V \rangle_D - p_A \langle \pi_V \rangle_A & p_D \langle \pi_V \rangle_D + p_A \langle \pi_V \rangle_A \end{pmatrix}. \quad (20)$$

Both axes of this density matrix use the H/V basis.

Additional Data

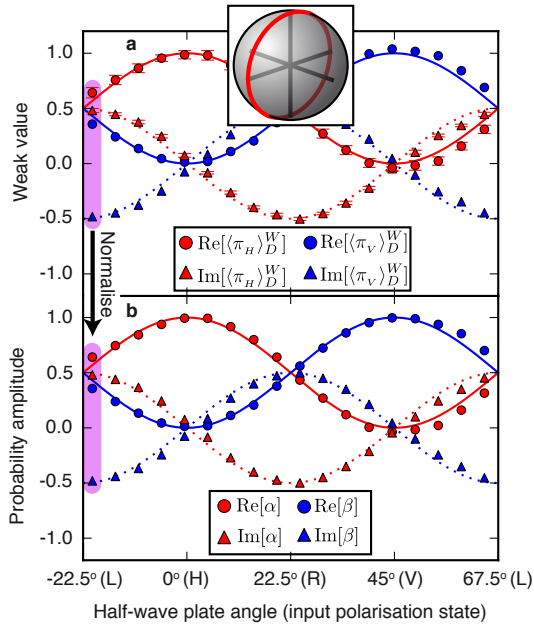


FIG. 5: Results of experiment 1 with elliptical probe states (quarter-wave plate fast axis 0°). **(a)** Measured weak values plotted as a function of half-wave plate angle. Error bars are shown only for the red points for clarity. **(b)** Real and imaginary components of the probability amplitudes determined by normalising the weak values of each test state, where $|\psi\rangle = \alpha|H\rangle + \beta|V\rangle$. For both panels, the solid lines are the theoretical predictions of the real components, and the dotted lines are the theoretical predictions of the imaginary components. **Inset:** A Poincaré sphere with the set of intended input states to directly measured indicated by the red line.

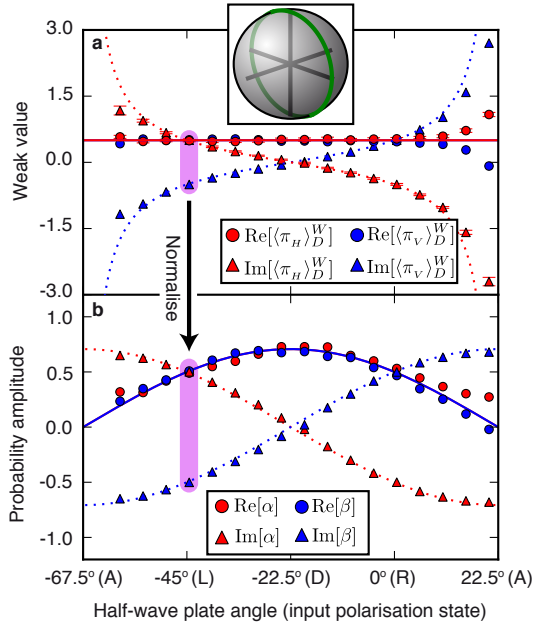


FIG. 6: Results of experiment 1 with elliptical probe states (quarter-wave plate fast axis 45°). **(a)** Measured weak values plotted as a function of half-wave plate angle. Error bars are shown only for the red points for clarity. **(b)** Real and imaginary components of the probability amplitudes determined by normalising the weak values of each test state, where $|\psi\rangle = \alpha|H\rangle + \beta|V\rangle$. For both panels, the solid lines are the theoretical predictions of the real components, and the dotted lines are the theoretical predictions of the imaginary components. **Inset:** A Poincaré sphere with the set of intended input states to directly measured indicated by the green line.